catalysts

MDPI

Article

A Comprehensive Assessment of Catalytic Performances of Mn_2O_3 Nanoparticles for Peroxymonosulfate Activation during Bisphenol A Degradation

Li Chen [1,2], Wanyi Fu [1,3,*], Congyu Hou [1,2], Yulong Yang [1,2] and Xihui Zhang [1,2,*]

1 Tsinghua Shenzhen International Graduate School, Tsinghua University, Shenzhen 518055, China; fenglin1129@163.com (L.C.); houcy17@mails.tsinghua.edu.cn (C.H.); yangyl19@mails.tsinghua.edu.cn (Y.Y.)
2 School of Environment, Tsinghua University, Beijing 100084, China
3 Tsinghua-Berkeley Shenzhen Institute, Tsinghua University, Shenzhen 518055, China
* Correspondence: fu.wanyi@sz.tsinghua.edu.cn (W.F.); zhangxh@sz.tsinghua.edu.cn (X.Z.)

Abstract: Catalytic performances of Mn_2O_3 nanoparticles for peroxymonosulfate (PMS) activation in bisphenol A (BPA) degradation were comprehensively investigated in this study. Experimental results showed that 10 mg/L BPA could be 100% degraded within 20 min with the dosages of 0.2 g/L Mn_2O_3 and 0.1 mM PMS. Moreover, Mn_2O_3 showed remarkable activity in activation of PMS and excellent adaptability in various real water matrices, including river water, tap water and secondary effluents. Based on the radical detection and scavenging experiments, it was found that both radical and non-radical oxidation contributed to the degradation of BPA and $^1O_2$ was the dominant species in the degradation compared to $^{\bullet}OH$, $SO_4^{\bullet-}$ and $O_2^{\bullet-}$. A total of 15 transformation products were identified by LC/MS-MS during BPA degradation in the Mn_2O_3/PMS system, and degradation pathways via three routes are proposed. Compared with lab-made catalysts reported in the literature, the Mn_2O_3 catalyst demonstrated its superiority in terms of its high TOC removal, low PMS consumption and fast degradation rate for BPA.

Keywords: peroxymonosulfate activation; Mn_2O_3 catalyst; bisphenol A; catalytic oxidation; singlet oxygen

Citation: Chen, L.; Fu, W.; Hou, C.; Yang, Y.; Zhang, X. A Comprehensive Assessment of Catalytic Performances of Mn_2O_3 Nanoparticles for Peroxymonosulfate Activation during Bisphenol A Degradation. *Catalysts* **2021**, *11*, 993. https://doi.org/10.3390/catal11080993

Academic Editors: Juan García Rodríguez and Silvia Álvarez-Torrellas

Received: 30 July 2021
Accepted: 17 August 2021
Published: 18 August 2021

1. Introduction

Bisphenol A (BPA) is classified as one of the endocrine-disrupting chemicals (EDCs) due to its estrogenic effect on human bodies [1]. The widespread use of BPA has resulted in its ubiquity in the natural environment [2,3] and even in drinking water [4,5]. Previous studies have reported the presence of BPA in human blood, urine and tissues, which might cause thyroid hormone disruption, heart diseases, cardiovascular disease and cancers [6,7]. BPA concentrations in WWTP effluent and surface waters were found to range from several ng/L to hundreds of μg/L [8–10]. It is of great significance to develop robust processes to remove BPA from aquatic environments.

In the last decade, PMS-based AOPs have been proposed for removal of organic contaminants, especially for the hazardous and refractory compounds (e.g., BPA) [1,11]. As well as sulfate radicals ($SO_4^{\bullet-}$), which have high redox potential, independence in pH and longer life times than hydroxyl radicals ($^{\bullet}OH$) [12], singlet oxygen ($^1O_2$) has been reported to play an important role in the degradation of organic pollutants [13,14] in PMS-based AOPs. Transition mental ions or oxides are used to activate PMS because they require less energy and have high reactivity [15]. Cobalt-based catalysts are one of the most effective activators for PMS [16,17]. However, the toxicity, high price and restricted availability of cobalt limit the applications of cobalt-based catalysts [18].

In contrast, manganese-based activators for PMS have gained increasing attenti on [11,19–24] because of their unique advantages [25], i.e., relatively lower toxicity than

Co, Cu and Zn; variable valence; high natural abundance in the earth; and environmental friendliness. Many reported manganese-based materials are doped with multiple transition metals (e.g., Fe, Co, Cu, Al, Zn, La and Ce) to enhance the catalytic activities for degradation of various recalcitrant organics. Materials such as $LaCo_{1-x}Mn_xO_3$ [26], $MnO_2/ZnFe_2O_4$ [27] and Ce/Mn_2O_3 [28] have been used as PMS activators for phenol degradation. Pharmaceutical and personal care products (PPCPs) are degraded by PMS activated by Co_3MnFeO_6 [29], $CuS/Fe_2O_3/Mn_2O_3$ [30] and Mn/Co_3O_4 [31]. CoMnAl [20] and $Mn_{1.8}Fe_{1.2}O_4$ [32] are used for the activation of PMS in degradation of EDCs. Furthermore, dyes are also decontaminated by PMS using α-MnO_2/palygorskite [33] and $MnO_2/MnFe_2O_4$ [34] as activators. Although the above materials are reported to have high catalytic abilities for PMS in the degradation of organic pollutants, harsh and precise conditions are required for the synthesis, limiting the possibilities for mass production and industrial applications.

In the past decade, most researchers have made efforts towards the synthesis of novel, complex and composite manganese-based catalysts, and few studies have focused on the usage of pure manganese oxides (MnO_x, i.e., MnO, MnO_2, Mn_2O_3 and Mn_3O_4) as PMS activators for the degradation of organic contaminants. MnO_x, comprised of elements that are abundant in the earths, has been commercially exploited from minerals or proficiently synthesized and used in the fields of chemical engineering and battery and steel production [35,36]. Therefore, MnO_x has the highest potential for practical application compared to other lab-made catalysts since it can be mass produced. Saputra et al. have studied MnO_2 and lab-made MnO, Mn_2O_3 and Mn_3O_4 as activators for PMS in the degradation of phenol, and the results showed that Mn_2O_3 had the highest activity [37]. However, to the best of our knowledge, no work has been conducted to explore the catalytic performance of Mn_2O_3 as a PMS activator for the degradation of BPA.

In this study, Mn_2O_3 catalysts with different particle sizes were purchased and their feasibility as activators for PMS was comprehensively assessed. The main objectives of this study were to: (i) investigate the influence of initial reaction parameters (BPA concentration, PMS/catalyst dosage, pH) and the presence of common co-existing ions, organic matter and other emerging organic contaminants; (ii) identify the major radical species, degradation pathways and mechanisms; and (iii) assess the stability and reusability of Mn_2O_3 catalysts and the toxicity of byproducts. The comprehensive assessment of the catalytic performance of available Mn_2O_3 for PMS activation during BPA degradation in this work proves the practicability of Mn_2O_3 for real water treatment.

2. Results and Discussion

2.1. Effects of Particle Sizes on Degradation of BPA in Mn_2O_3/PMS System

Nano- and microparticles of Mn_2O_3 were chosen for size-dependent studies on BPA removal. As revealed in Figure 1a, the adsorption of BPA was little affected by the size of the Mn_2O_3 catalyst. The adsorption rate was less than 10% of the total BPA. The low BPA adsorption capacity indicates that BPA does not occupy active sites for PMS activation on the surface of Mn_2O_3. As Figure 1b shows, with smaller particle sizes, the degradation rate of BPA became faster. The pseudo-first-order rate constants (k) were 0.1044 min^{-1}, 0.0557 min^{-1} and 0.0201 min^{-1} for Mn_2O_3 catalysts with particle sizes of 55 nm, 136 nm and 1894 nm, respectively. The reaction stoichiometric efficiency (RSE) was used to further evaluate the utilization efficiency of PMS for nano- and microparticles of Mn_2O_3 [38]. RSE was defined as the molar concentration ratio of oxidized BPA (Δ[BPA]) to consumed PMS (Δ[PMS]). The RSE values were 36%, 33% and 23% for degradation processes using Mn_2O_3 with particle sizes of 55 nm, 136 nm and 1894 nm, respectively. Mn_2O_3 with a smaller size greatly improved the catalytic activity by providing more accessible reactive sites and activated PMS to the greatest degree. For the following experiment, Mn_2O_3 with an average particle size of 55 nm was used.

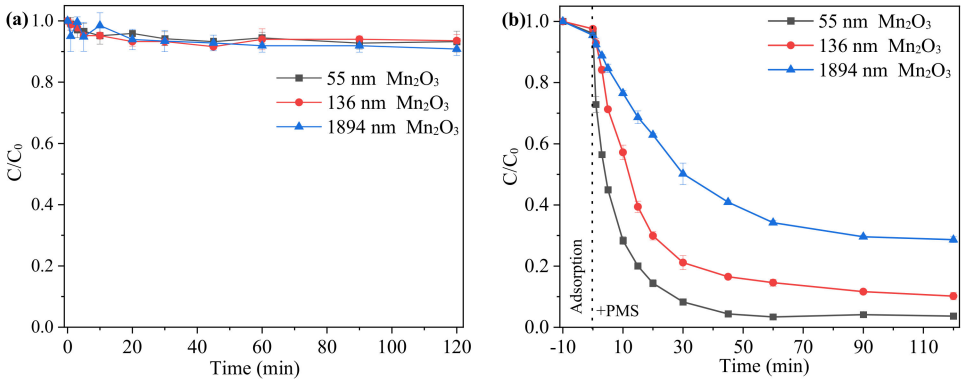

Figure 1. Effects of catalyst sizes on BPA removal efficiencies in (**a**) adsorption by Mn_2O_3 and (**b**) degradation by the Mn_2O_3/PMS system. Reaction conditions: $[BPA]_0$ = 10 mg/L, $[PMS]_0$ = 0.5 mM, $[Mn_2O_3]_0$ = 0.1g/L, initial pH = 7.0 ± 0.2.

2.2. Effect of PMS and Catalyst Dosages

BPA degradation as a function of PMS dosages (0.01–0.50 mM) was studied at a fixed Mn_2O_3 dosage (0.1 g/L). Detailed information for the linear equations and R^2 values is provided in Table S2. As shown in Figure 2, the degradation rate of BPA accelerated when the PMS dosage increased from 0.01 to 0.3 mM in the Mn_2O_3/PMS system, and the value of k increased from 0.0441 to 0.1360 min^{-1}. With low PMS dosages, active sites on the Mn_2O_3 surfaces could not be utilized effectively because insufficient PMS was a limiting factor on the reaction rate. However, a further increase in PMS concentration to 0.5 mM slightly decreased BPA degradation. When PMS concentration is high, the limited active sites for PMS on the surface of the Mn_2O_3 can gradually become saturated. Simultaneously, the excess amount of PMS can react with $SO_4^{\bullet-}$ and $^{\bullet}OH$ to form $SO_5^{\bullet-}$ (see Equations (1) and (2)). $SO_5^{\bullet-}$ has lower oxidation potential than $SO_4^{\bullet-}$, resulting in attenuated degradation of BPA [39,40]. Thus, 0.1 mM PMS was finally selected for the follow-up studies.

$$HSO_5^- + SO_4^{\bullet-} \rightarrow SO_5^{\bullet-} + SO_4^{2-} + H^+ \quad (1)$$

$$HSO_5^- + {}^{\bullet}OH \rightarrow SO_5^{\bullet-} + H_2O \quad (2)$$

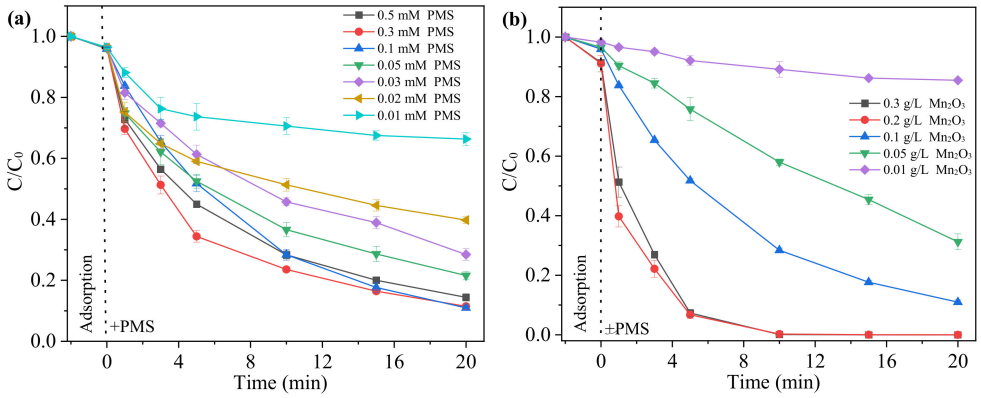

Figure 2. Effects of (**a**) PMS concentration and (**b**) Mn_2O_3 dosage on the degradation of BPA. (**a**) Reaction conditions: $[BPA]_0$ = 10 mg/L, $[PMS]_0$ = 0.01–0.5 mM, $[Mn_2O_3]_0$ = 0.1 g/L, initial pH = 7.0; (**b**) Reaction conditions: $[BPA]_0$ = 10 mg/L, $[PMS]_0$ = 0.1 mM, $[Mn_2O_3]_0$ = 0.01–0.3 g/L, initial pH = 7.0 ± 0.2.

Figure 2b shows that the increase of Mn_2O_3 dosage remarkably enhanced the degradation of BPA at a constant PMS dosage (0.1 mM). k values increased linearly from 0.0070 to 0.7500 min^{-1} when the Mn_2O_3 dosage increased from 0.01 to 0.30 g/L. The enhancement

of BPA degradation with higher Mn_2O_3 dosages may be attributable to there being more active sites available for PMS activation [41].

2.3. Influence of Water Matrix on the Degradation of BPA

2.3.1. Effect of pH

The initial pH of reaction solutions greatly impacts the degradation efficiency of BPA in PMS/catalyst systems due to its influence on the surface charge of catalysts, the fractions of PMS species and the speciation of organic compounds [13]. The effect of initial pH on the degradation of BPA is shown in Figure 3. It can be seen that Mn_2O_3 presented appreciable BPA degradation efficiency in the tested pH range. BPA could be 100% degraded in 20 min for pH 4.0–9.0 and fast kinetics were observed when the pH = 9.0. When the pH value was further increased to 10.8, only 93% of BPA was degraded in 20 min. The pK_{a1} and pK_{a2} values of PMS were 0 and 9.4, which shows that HSO_5^- was the dominant PMS species under the condition of pH < 9.4 and SO_5^{2-} at pH > 9.4 [42–44]. In acidic conditions (pH = 4.0), reactive oxygen species (ROS), such as $SO_4^{\bullet-}$ and $^{\bullet}OH$, can be scavenged by H^+ [45,46]. Moreover, H^+ attaches on the electronegative O–O group of PMS and increases the interfacial repulsion between PMS and Mn_2O_3 [47]. Both cases are detrimental to the catalytic performance, resulting in less degradation of BPA. When the initial pH value is increased to strongly alkaline (pH = 10.8), SO_5^{2-} becomes the main PMS species and the surface of Mn_2O_3 is negatively or positively charged because Mn_2O_3 has a point of zero charge (pH_{pzc}) at pH = 5.3 (Figure S1). In such cases, electron repulsion would reduce the interaction between SO_5^{2-} and the negative charged Mn_2O_3, leading to a lower degradation efficiency for BPA. At a pH of 9.0, PMS decomposes to HSO_5^- and SO_5^{2-} at similar concentrations [48], and PMS is activated under weak alkaline condition to form singlet oxygen ($^1O_2$) and superoxide anion radicals ($O_2^{\bullet-}$), which would accelerate the degradation of BPA [49,50]. Therefore, the highest degradation efficiencies for the PMS/Mn_2O_3 system were observed at neutral or weakly alkaline pH as shown in Figure 3.

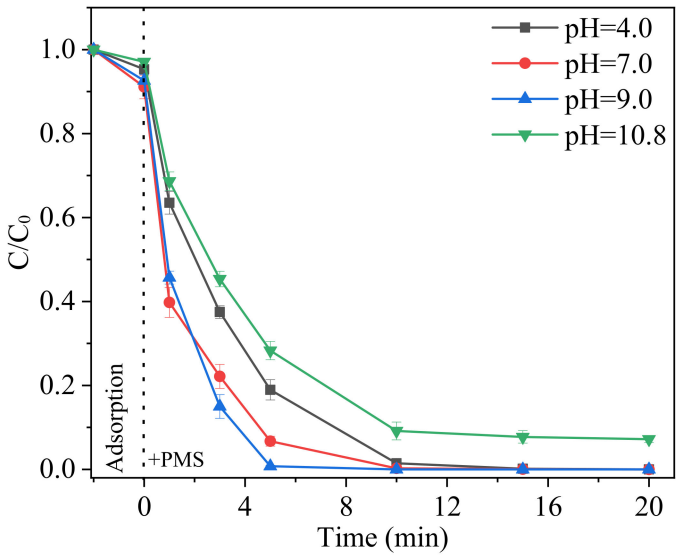

Figure 3. Effect of initial pH on BPA degradation; $[BPA]_0$ = 10 mg/L, $[PMS]_0$ = 0.10 mM and $[Mn_2O_3]_0$ = 0.2 g/L.

2.3.2. Effect of Co-existing Inorganic Ions

Real water contains various inorganic ions and types of natural organic matter (NOM). Figure S2 shows the effect of co-existing inorganic ions on BPA degradation in the Mn_2O_3/PMS system. As for inorganic anions, such as Cl^-, NO_3^- and HCO_3^-, in the range of 1–100 mM, no distinct inhibition on the removal rate of BPA was found. Compared to other anions, a high concentration of Cl^- can accelerate the BPA degradation. It has been reported that a high concentration of Cl^- will react with PMS to generate

active chlorine or hypochlorous species (i.e., $Cl^{\bullet}$, $Cl_2^{\bullet-}$ and $ClOH^{\bullet-}$), which accelerate the removal rate of BPA [51]. Similar results were presented by Dong et al. [15], who found that high concentration of Cl^- (0.1M) greatly improved the degradation of BPA in a PMS/$CuFe_2O_4$ system. In contrast, high concentrations of NO_3^- and HCO_3^- would slightly inhibit the degradation of BPA. This might be because HCO_3^- and NO_3^- can react with $^{\bullet}OH$ or $SO_4^{\bullet-}$ to form less reactive $CO_3^{\bullet-}$ and $NO_3^{\bullet}$, respectively [52]. Both Ca^{2+} and Mg^{2+} can accelerate BPA degradation because cations enable bridging between HSO_5^- and Mn_2O_3, leading to easier reduction of PMS for the formation of radicals and, finally, enhancing the oxidizing power of PMS [41].

2.3.3. Effects of HA and BPA Initial Concentrations

Humic acid (HA) is usually used as a representative of NOM in water [53]. As can be seen in Figure S2, the addition of HA greatly slowed down the degradation process of BPA, with k values decreasing from 0.5402 min^{-1} (without HA) to 0.0379 min^{-1} (with 20 mg/L HA). However, no obvious inhibitory effect on BPA removal was observed in the presence of 1 mg/L (100%) and 10 mg/L HA (92%). When further increasing the dosage of HA to 20 mg/L, the degradation rate of BPA decreased to 74% in 20 min.

In previous studies inform the literature, the degradation efficiency of BPA decreased from 78% to 52% with the addition of 10 mg/L HA in a CuO/PMS system [54] and from 88% to 59% with the addition of 5 mg/L HA in a $MnFe_2O_4$/PMS system [19]. The inhibitory effect of HA can be primarily attributed to its competition with BPA for ROS during the oxidation process and its competitive adsorption on the catalyst surface to occupy the accessible active sites for PMS [55]. Nevertheless, the influence of HA on BPA removal in the Mn_2O_3/PMS system seemed to be much milder than that found in previous research. Reasons for this phenomenon need to be elucidated in future studies for a better understanding of the interaction mechanism between HA and Mn_2O_3.

Usually, the concentrations of BPA in real water range from ng/L to μg/L and BPA coexists with other organics [56]. In order to further test the potential of the Mn_2O_3/PMS system in field applications, the degradation of 0.1 mg/L BPA in the presence of 10 mg/L HA was implemented. As Figure 4a shows, the BPA could be totally degraded by the Mn_2O_3/PMS system even when the concentration of coexisting HA was 100 times higher than that of BPA. Moreover, as Figure 4b shows, complete BPA removal could be achieved at initial BPA concentrations of 0.1, 1 and 10 mg/L, while for the 20 and 30 mg/L BPA, the removal rates were 90% and 78% in 20 min, respectively. The results demonstrate that the Mn_2O_3/PMS system is promising for the removal of trace amounts of BPA in real water.

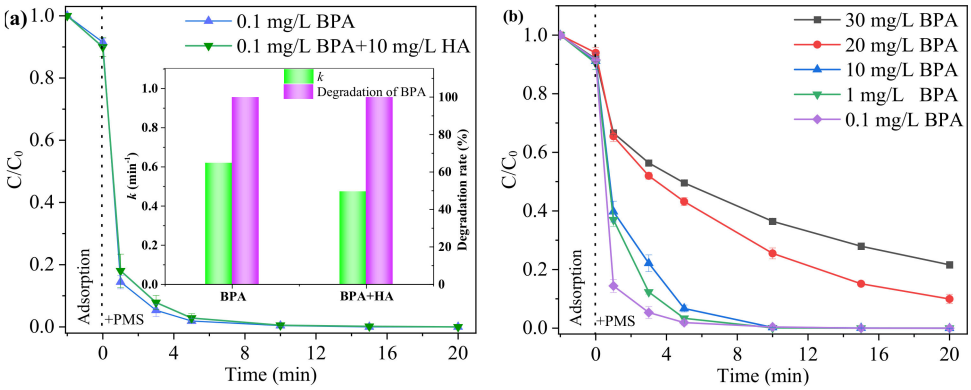

Figure 4. Effects of (**a**) HA and (**b**) BPA initial concentration on BPA degradation. Reaction conditions: $[PMS]_0$ = 0.10 mM, $[Mn_2O_3]_0$ = 0.2 g/L, initial pH = 7.0 ± 0.2.

2.3.4. Degradation of BPA in Real Water and in the Presence of other EOCs

In order to further verify the efficiency of Mn_2O_3/PMS in the degradation of BPA in real water, river water (RW), secondary effluent from a wastewater plant (SE) and tap water (TW) spiked with 10 mg/L BPA were used for tests. Table S1 lists the water quality

parameters of these three types of real water. As Figure 5a shows, the BPA removal rates were 99%, 97% and 94% in 20 min for RW, TW and SE, respectively. The minor inhibitory effect may have been due to the co-existing complex components in real water. The lowest efficiency of BPA degradation was found in treating the SE, which may have been caused by the higher concentrations of TOC and inorganic ions in SE than in TW and RW. A higher degradation rate of BPA in RW was found compared to TW. This might have been caused by enhanced oxidation due to the existence of higher concentrations of Ca^{2+} and Mg^{2+} in RW.

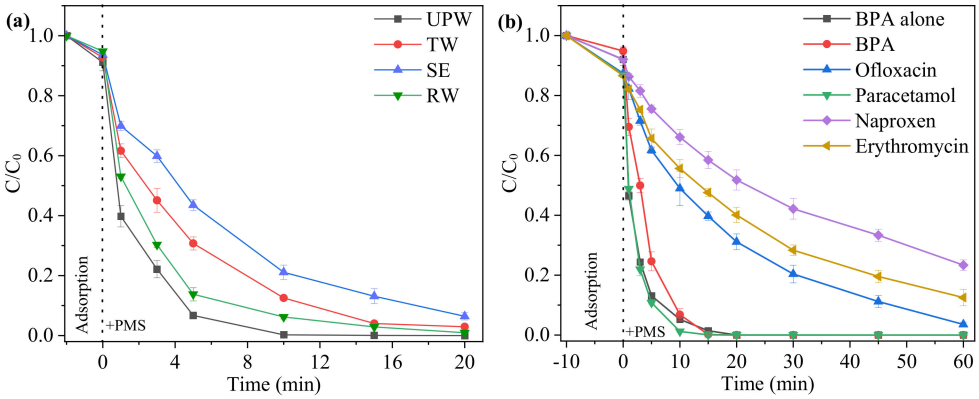

Figure 5. Degradation of BPA (**a**) in different water matrices and (**b**) with various emerging organics in the Mn_2O_3/PMS system. (**a**) Reaction conditions: $[BPA]_0$ = 10 mg/L, $[PMS]_0$ = 0.10 mM, $[Mn_2O_3]_0$ = 0.2 g/L, initial pH = 7.0 ± 0.2. (**b**) Reaction conditions: $[BPA]_0$ = $[Ofloxacin]_0$ = $[Paracetamol]_0$ = $[Naproxen]_0$ = $[Erythromycin]_0$ = 5 mg/L, $[PMS]_0$ = 0.10 mM, $[Mn_2O_3]_0$ = 0.2 g/L, initial pH = 7.0 ± 0.2.

The catalytic activity of the Mn_2O_3 with PMS activation was also evaluated for its potential to degrade a variety of frequently detected emerging organic contaminants (EOCs). Two antibiotics (erythromycin and ofloxacin) and two inflammatory drugs (paracetamol and naproxen) were selected and spiked into UPW with BPA as a mixture for tests. Figure 5b shows that up to 100%, 100%, 96%, 87% and 77% of the BPA, paracetamol, ofloxacin, erythromycin and naproxen, respectively, were degraded within 60 min. Surprisingly, compared to BPA alone, the degradation efficiency of Mn_2O_3/PMS towards BPA was not affected by the presence of other organic pollutants. Hence, the Mn_2O_3/PMS oxidation process has potential for the decontamination of various water matrices.

2.4. Detection of Reactive Species and Possible Generation Mechanisms

2.4.1. Identification of Reactive Species

According to the literature [12], hydroxyl radicals ($^{\bullet}OH$), sulfate radicals ($SO_4^{\bullet-}$), singlet oxygen ($^1O_2$) and superoxide anion radicals ($O_2^{\bullet-}$) may coexist in a PMS activation system. A series of selective radical quenching tests were implemented in order to identify the predominant ROS involved in the Mn_2O_3/PMS system. MeOH and TBA were adopted as quenchers as MeOH has a high reactivity to both $^{\bullet}OH$ ($k_{\bullet OH}$ = 9.7 × 10^8 M^{-1} s^{-1}) and $SO_4^{\bullet-}$ ($k_{SO4\bullet-}$ = 1.6 × 10^7 M^{-1} s^{-1}) while TBA without α-H mainly reacts with $^{\bullet}OH$ ($k_{\bullet OH}$ = (3.8–7.6) × 10^8 M^{-1} s^{-1}) but is inefficient for the scavenging of $SO_4^{\bullet-}$ ($k_{SO4\bullet-}$ = (4.0–9.1)×10^5 M^{-1} s^{-1}) [57]. p-BQ with a first-order reaction rate constant $k_{O2\bullet-}$ of 9.6×10^8 M^{-1} s^{-1} was selected as a scavenger of $O_2^{\bullet}$ [58]. Additionally, FFA exhibited high reactivity with $^1O_2$ (k_{1O2} = 1.2 × 10^8 M^{-1} s^{-1}) and was selected as the scavenger for $^1O_2$ [12].

Figure 6a shows that when MeOH was added to the Mn_2O_3/PMS/BPA system with a molar ratio of MeOH/PMS = 200/1000, the rate constant k of the BPA degradation process decreased from 0.5454 min^{-1} (without quencher) to 0.3374 min^{-1} and 0.2478 min^{-1}, respectively, indicating that $^{\bullet}OH$ and $SO_4^{\bullet-}$ existed in the oxidation reaction. Meanwhile, addition of TBA (with a molar ratio of TBA/PMS = 200/1000) resulted in no distinct

changes in the degradation of BPA, indicating that •OH contributes little in the oxidation reaction. Based on the quenching results for MeOH and TBA, both •OH and $SO_4^{\bullet-}$ existed in the oxidation system but $SO_4^{\bullet-}$ plays a more important role than •OH.

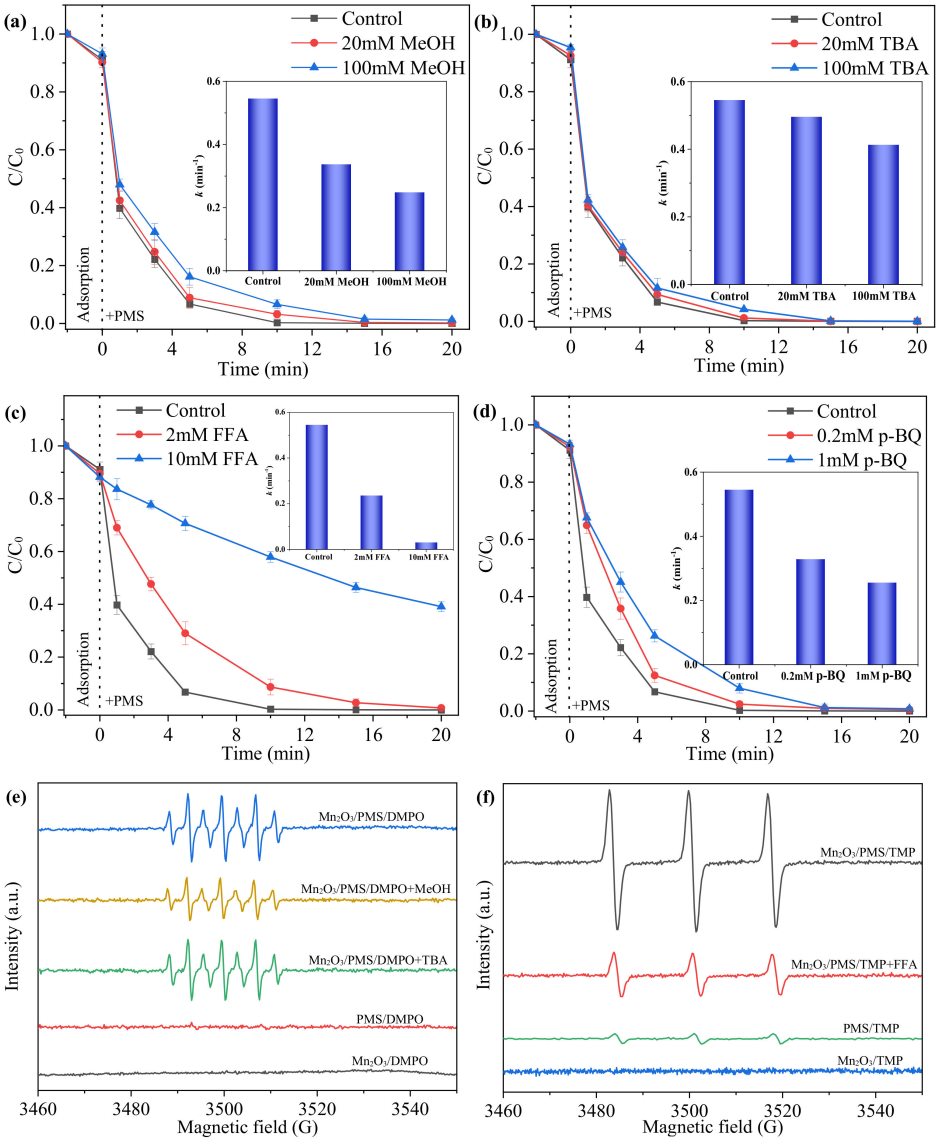

Figure 6. Influence of quenching agents on the degradation efficiency of BPA: (**a**) MeOH, (**b**) TBA, (**c**) FFA and (**d**) p-BQ. EPR spectrum of the Mn_2O_3/PMS in the presences of (**e**) DMPO and (**f**) TMP. Reaction conditions: $[BPA]_0$ = 10 mg/L, $[PMS]_0$ = 0.1 mM, $[Mn_2O_3]_0$ = 0.2 g/L, [MeOH] = 0.1 M, [TBA] = 0.1 M, [FFA] = 10 mM, [DMPO] = 10 mM, [TMP] = 1 mM, initial pH = 7.0 ± 0.2.

Figure 6c shows that with the increasing concentrations of FFA, the degradation efficiency of BPA was inhibited significantly. The *k* values decreased to 0.2365 min^{-1} and 0.0305 min^{-1}, respectively, with a molar ratio of FFA/PMS = 20/100, since FFA can also scavenge •OH with a first-order reaction rate constant $k_{\bullet OH}$ of 1.5 × 10^{10} M^{-1} s^{-1} [12]. Comparing the results for FFA and TBA, it can be seen that the inhibition effect of FFA contributed to quenching $^1O_2$ rather than •OH. As shown in Figure 6d, the *k* values decreased to 0.3286 min^{-1} and 0.2558 min^{-1}, respectively, with a molar ratio of p-BQ/PMS = 2/10, which indicated the existence of $O_2^{\bullet-}$ in the Mn_2O_3/PMS system. Thus, it is reasonable to conclude that $^1O_2$, $O_2^{\bullet-}$, $SO_4^{\bullet-}$ and •OH coexisted in the reaction system and that $^1O_2$ played a much more crucial role than $O_2^{\bullet-}$, $SO_4^{\bullet-}$ and •OH in the degradation of BPA.

Furthermore, ROS species were confirmed by EPR analysis. DMPO was used as the spin trapping agent for $SO_4^{\bullet-}$, $^{\bullet}OH$ and $O_2^{\bullet-}$ while TMP was used for $^1O_2$. As shown in Figure 6e, when both Mn_2O_3 and PMS were present, the signal for 5,5-dimethylpyrroline-(2)-oxyl-(1) (DMPOX) with a narrow seven-line (1:2:1:2:1:2:1) spectrum was observed. It has been reported that DMPOX is generated from the excessive oxidation of DMPO by strong oxidizing substances, such as $SO_4^{\bullet-}$ and $^{\bullet}OH$ [59]. This indicated the presence of $SO_4^{\bullet-}$ and $^{\bullet}OH$ in the reaction system, though no obvious signals of DMPO-$SO_4^{\bullet-}$ and DMPO-$^{\bullet}OH$ adducts were detected [60]. Instead, the main reason would have been that the oxidation rate of DMPO was much faster than that of trapping radicals in our system [59]. Therefore, the peak intensity of DMPOX was used to indirectly reflect the number of free radicals [59]. As can be seen in Figure 6e, the intensity of the DMPOX signals only slightly decreased when TBA was added, but a relatively more obvious decrease was observed when MeOH was added. This result further demonstrated that $SO_4^{\bullet-}$ played a more important role than $^{\bullet}OH$ in the degradation of BPA. As shown in Figure 6f, a strong triplet signal displayed as 1:1:1 in the EPR pattern for TMP-$^1O_2$ was found in the Mn_2O_3/PMS system, and only a small amount of $^1O_2$ was formed through self-decomposition, indicating that $^1O_2$ was formed during the reaction. When FFA was added to the reaction system, the intensity of TMP-$^1O_2$ significantly decreased, which further demonstrated that a large number of $^1O_2$ existed in the Mn_2O_3/PMS system. No obvious signal for $O_2^{\bullet-}$ was detected, indicating that $O_2^{\bullet-}$ was not generated in the oxidation system or that its concentration was too low to be detected [61]. However, according to the results of the quenching experiments, $O_2^{\bullet-}$ was formed during the reaction process; therefore, the main reason for its absence in the EPR signals was its low concentration.

2.4.2. Roles of Manganese and Oxygen Species

In order to better understand the activation mechanism of Mn_2O_3 catalysts, the surface element composition and oxidation state of the Mn_2O_3 catalyst were further investigated with XPS. Figure 7a shows the varying valence of the Mn element before and after the reaction. Two characteristic broad peaks, the Mn 2p1/2 peak at 653.5 eV and the Mn 2p3/2 peak at 641.7 eV, were observed. The latter is consistent with the spectrum of Mn^{3+} oxidation states of Mn as reported in [62]. Three peaks with binding energies of 640.7 eV, 641.7 eV and 643.6 eV were fitted for the Mn 2p3/2 spectrum, corresponding to Mn^{2+}, Mn^{3+} and Mn^{4+}, respectively [63], the relative intensities of which were 23:57:20 in fresh Mn_2O_3. After the reactions, the relative intensities of $Mn^{2+}/Mn^{3+}/Mn^{4+}$ changed to 22:44:34, which suggests that redox reactions between the $Mn^{2+}/Mn^{3+}/Mn^{4+}$ occurred during the PMS activation process. The interaction between Mn_2O_3 and PMS was further demonstrated by in situ Raman spectroscopy. As shown in Figure S3, compared with the pure PMS solution, the characteristic vibration peak of the O-O of the HSO_5^- species in the Mn_2O_3/PMS suspension clearly red-shifted from 882 cm^{-1} to 880 cm^{-1} because the interaction between PMS and Mn_2O_3 weakened the electron density of the S-O bond [41]. Furthermore, a new peak appeared at 836 cm^{-1}, which is the characteristic feature of surface peroxo species [64], as a consequence of the strong affinity between the active sites of Mn_2O_3 and PMS [65].

As leached Mn can be detected after the degradation of BPA, it is necessary to verify the roles of homogeneous and heterogeneous catalysis in the Mn_2O_3/PMS system. Thus, the degradation of BPA by homogenous catalysis (Mn^{3+}) was carried out under identical reaction conditions except that catalysts were 0.14 g/L Mn^{3+} (same Mn content as 0.2 g/L Mn_2O_3). As the results in Figure S4 show, the BPA degradation efficiency in the Mn^{3+}/PMS system was 36% in 60 min, much lower and slower than that achieved by the heterogeneous Mn_2O_3 catalysts (100% in 20 min). Furthermore, the potential presence of Mn^{3+} in the suspension was verified via UV-vis spectroscopy. As revealed in Figure S5, no obvious absorbance peak was found for the Mn^{3+}–sodium pyrophosphate complex, which indicates the presence of Mn^{3+} [66], during the reaction period. Thus, the degradation of BPA in the Mn_2O_3/PMS system was mostly by heterogeneous catalysis instead of homogeneous catalysis.

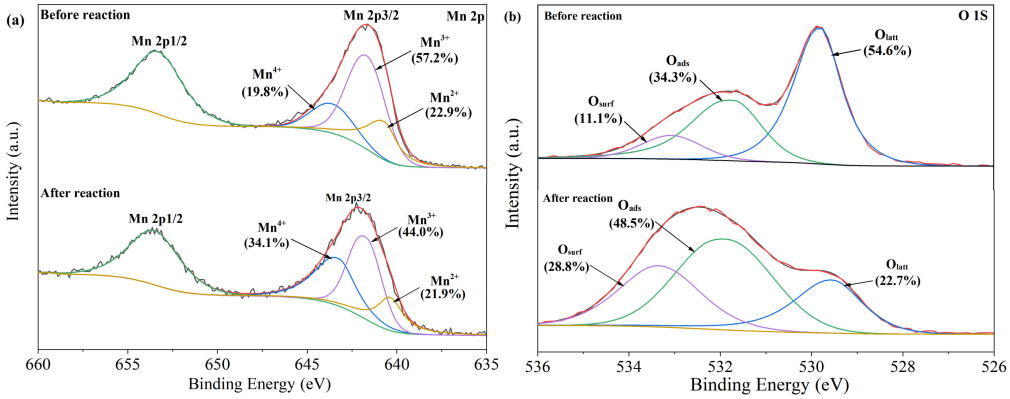

Figure 7. XPS characterization of fresh Mn_2O_3 and used Mn_2O_3: (**a**) Mn 2p, (**b**) O 1s.

It has been reported that oxygen species on catalyst surfaces affect their catalytic and oxidative reactivity [67]. Figure 7b shows the high-resolution spectra of O 1s for fresh and used Mn_2O_3. All the O 1s spectra of the surface oxygen species could be deconvoluted into three types. The peaks located at 529.8 eV, 531.7 eV and 533.1 eV were assigned to lattice oxygen (O_{latt}) with metal, adsorbed oxygen or surface hydroxyl groups (O_{ads}) and adsorbed H_2O (O_{surf}), respectively [68]. The changes in the area percentages of O_{latt}, O_{ads} and O_{surf} before and after the reaction suggested that O_{latt}, O_{ads} and O_{surf} were all involved in the catalytic oxidation process. The increase of O_{ads} can be attributed to the formation of metal–OH groups during the reaction, and the decrease of O_{latt} can be explained as the oxidation of O_{latt} to O_2 through the reduction of Mn^{n+1} to Mn^{n+} [42]. The enhancement of O_{ads} could greatly accelerate the dispersion of catalysts in solutions by further increasing the accessible reactive sites. Moreover, hydroxyl groups on the surface of the Mn_2O_3 can activate PMS to generate reactive radicals [69]. It has been reported that O_{ads} is associated with defect sites (oxygen vacancies, O_{vac}) with low oxygen coordination [13,54,70]. Oxygen vacancy concentration is reflected by the XPS peak area ratio (R) of O_{ads} to O_{latt} [71]. The values of R for the fresh and used Mn_2O_3 were 0.6 and 2.1, respectively, indicating that the surface oxygen vacancy concentration increased greatly during the reaction process. Furthermore, oxygen vacancies tend to adsorb oxygen because of the defect structure, forming active oxygen species on the surfaces of catalysts [16]. Meanwhile, during the reaction process, O_{latt} can be released and form O_{vac}, which then transforms into active oxygen (O *) and further reacts with PMS to generate $^1O_2$ [72]. What's more, the presence of O_{vac} can also activate O_{ads} to form $^1O_2$ [73]. Thus, the generation of O_{vac} greatly enhanced the redox capability of the Mn_2O_3 and improved the remarkable catalytic activation performance for PMS and BPA degradation in the Mn_2O_3 suspension.

2.4.3. Hypothetic Mechanisms of Reactive Oxygen Species Generation

Based on the above results and analysis, catalytic mechanisms in the Mn_2O_3/PMS system can be proposed. The first mechanism is the radical oxidation process. PMS could conjunct with the surface-hydroxylated Mn(II) and Mn(III) and obtain one electron from catalysts to generate $SO_4^{\bullet-}$ according to Equations (3) and (4). On the other hand, PMS could also give one electron to a catalyst to generate $SO_5^{\bullet-}$, while Mn(III)/Mn(IV) could be transformed to Mn(II)/Mn(III) (Equations (5) and (6)). Furthermore, $SO_4^{\bullet-}$ could react with H_2O or OH^- to produce $^{\bullet}OH$ (Equations (7) and (8)). According to previous research [33,52,74], $O_2^{\bullet-}$ can also be formed by reactions as shown in Equations (9) and (11). The dissolved oxygen can obtain one electron from an oxygen vacancy and form $O_2^{\bullet-}$ [74] (Equation (13)).

$$\equiv Mn(II)\text{-}OH + HSO_5^- \rightarrow \equiv Mn(II)\text{-}(O)OSO_3^- + H_2O \rightarrow \equiv Mn(III)\text{-}OH + SO_4^{\bullet-} + OH^- \quad (3)$$

$$\equiv Mn(III)\text{-}OH + HSO_5^- \rightarrow \equiv Mn(III)\text{-}(O)OSO_3^- + H_2O \rightarrow \equiv Mn(IV)\text{-}OH + SO_4^{\bullet-} + OH^- \quad (4)$$

$$\equiv Mn(III)\text{-}(O)OSO_3^- + H_2O \rightarrow \equiv Mn(II)\text{-}OH + SO_5^{\bullet -} + H^+ \quad (5)$$

$$\equiv Mn(IV)\text{-}OH + HSO_5^- \rightarrow \equiv Mn(IV)\text{-}(O)OSO_3^- + H_2O \rightarrow \equiv Mn(III)\text{-}OH + SO_5^{\bullet -} + H^+ \quad (6)$$

$$SO_4^{\bullet -} + H_2O \rightarrow {}^{\bullet}OH + H^+ + SO_4^{2-} \quad (7)$$

$$SO_4^{\bullet -} + OH^- \rightarrow {}^{\bullet}OH + SO_4^{2-} \quad (8)$$

$$HSO_5^- + H_2O \rightarrow H_2O_2 + HSO_4^- \quad (9)$$

$$H_2O_2 + {}^{\bullet}OH \rightarrow HO_2^{\bullet} + H_2O \quad (10)$$

$$HO_2^{\bullet -} \rightarrow O_2^{\bullet -} + H^+ \quad (11)$$

$$2SO_5^{\bullet -} \rightarrow 2\,SO_4^{\bullet -} + O_2 \quad (12)$$

$$O_2 + e^- \rightarrow O_2^{\bullet -} \quad (13)$$

The second mechanism is the non-radical oxidation process. It has been reported that $^1O_2$ can be produced during the self-decomposition of PMS (Equation (14)) [73]. Furthermore, $^1O_2$ can be generated not only from reactions involving $^{\bullet}OH$ and $O_2^{\bullet -}$ (Equations (15)–(17)) [33,75], but also from the reaction between the HSO_5^- and O * that were converted from O_{latt} (Equations (18) and (19)). Based on the above analysis, a possible catalytic mechanism for the generation of ROS in the Mn_2O_3/PMS system is shown in Figure 8.

$$HSO_5^- + SO_5^{2-} \rightarrow HSO_4^- + SO_4^{2-} + {}^1O_2 \quad (14)$$

$$2{}^{\bullet}OH \rightarrow 1/2\,{}^1O_2 + H_2O \quad (15)$$

$$O_2^{\bullet -} + {}^{\bullet}OH \rightarrow {}^1O_2 + OH^- \quad (16)$$

$$2O_2^{\bullet -} + 2H^+ \rightarrow {}^1O_2 + H_2O_2 \quad (17)$$

$$O_{latt} \rightarrow O\,* \quad (18)$$

$$O\,* + HSO_5^- \rightarrow HSO_4^- + {}^1O_2 \quad (19)$$

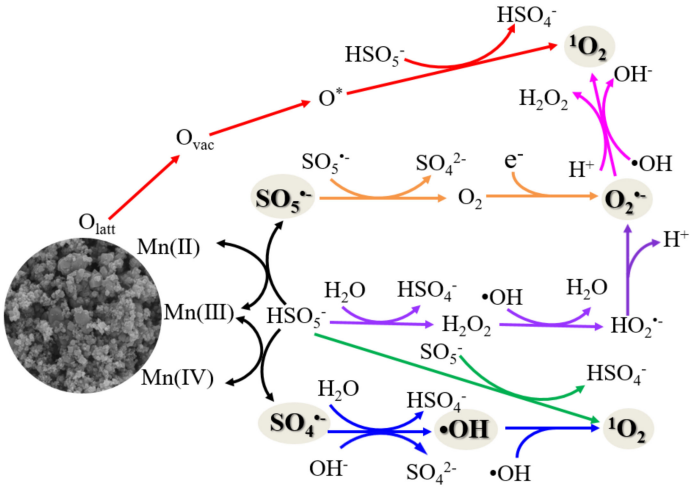

Figure 8. Hypothetic mechanisms of reactive oxygen species generation in the Mn_2O_3/PMS system.

2.5. Degradation Pathways of BPA in the Mn_2O_3/PMS System

Transformation products (TPs) generated during the degradation of BPA were detected by HPLC/MS/MS in full-scan mode. The total ion current (TIC) chromatogram and mass spectra are provided in Figure S6. Fifteen main TPs were identified and the detailed information is summarized in Table S3. Based on the m/z values of the various TPs and

the experimental results of this work, reaction pathways with three routes are proposed in Figure 9.

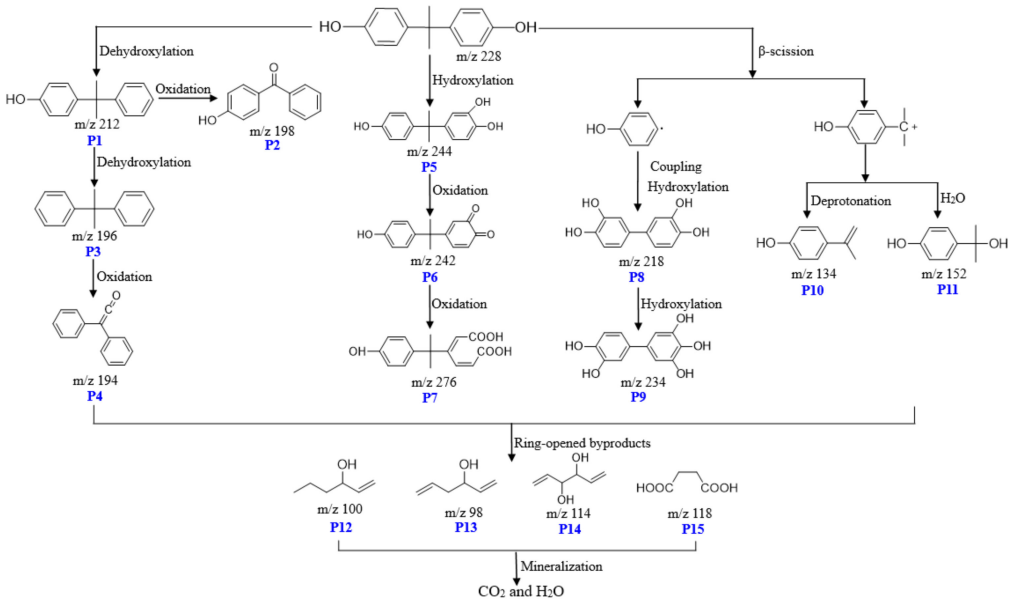

Figure 9. Proposed transformation pathways of BPA in the Mn_2O_3/PMS system.

First, the generated $SO_4^{\bullet-}$ or $^{\bullet}OH$ might attach the C-O bond via a dehydroxylation pathway and result in the generation of 4-(2-phenylpropan-2-yl)phenol (P1, m/z = 211) [15]. Then, P1 could either be further oxidized to (4-hydroxyphenyl)(phenyl)methanone (P2, m/z = 197)) or undergo dehydroxylation to propane-2,2-diyldibenzene (P3, m/z = 195). Later, P3 could be further oxidized into 2,2-diphenylethen-1-one (P4, m/z = 193). It has been reported that $^1O_2$ is a selectively electrophilic ROS that can oxidize electro-rich compounds such as phenols, olefins and aromatic hydrocarbons [76]. In addition, $^1O_2$ can decompose BPA rapidly through hydroxylation and β-scission reactions, which can produce 4-(2-(4-hydroxyphenyl)propan-2-yl)benzene-1,2-diol (P5, m/z = 243), phenol radicals and cationic 4-isopropylphenol [76,77]. P5 can be further oxidized into 4-(2-(4-hydroxyphenyl)propan-2-yl)cyclohexa-3,5-diene-1,2-dione (P6, m/z = 241) and (2E,4Z)-3-(2-(4-hydroxyphenyl)propan-2-yl)hexa-2,4-dienedioic acid (P7, m/z = 275).

As for the degradation route via β-scission, the formed phenol radicals could transform into [1,1′-biphenyl]-3,3′,4,4′-tetraol (P8, m/z = 217) through coupling and hydroxylation since radical couplings are common reactions for the oxidation of phenolic compounds [78]. [1,1′-biphenyl]-3,3′,4,4′,5-pentaol (P9, m/z = 233) can be obtained through the hydroxylation of P8. The cationic 4-isopropylphenol formed by β-scission could also trigger a series of substitution and elimination reactions. For instance, cationic 4-isopropylphenol can be subject to deprotonation and form 4-(prop-1-en-2-yl)phenol (P10, m/z = 133) [79]; moreover, it can also form 2-(4-hydroxypheny)-propanol-2-ol (P11, m/z = 151) through the substitution of a proton of water [80]. Subsequently, ring-rupturing reactions could occur and form unsaturated aromatic hydrocarbons and carboxylic acids, such as hex-1-en-3-ol (P12, m/z = 99), hexa-1,5-dien-3-ol (P13, m/z = 97), hexa-1,5-diene-3,4-diol (P14, m/z = 113) and succinic acid (P15, m/z = 117), which would finally transform to CO_2 and H_2O.

Furthermore, the biological toxicity of TPs was investigated by measuring the oxygen uptake rate (OUR) of activated sludge after adding the BPA solutions before and after treatment. A high inhibited OUR percentage indicated high toxicity. As shown in Figure S7, the untreated BPA solution caused 10% inhibition, but the percentage decreased to 2.5% after the 5 min reaction. Meanwhile, the BPA and TOC removal rates were 93% and 53% during the first 5 min reaction, respectively (see Figure S6). The reason for the

sharp decrease in toxicity would mainly be due to the high degradation of BPA and transformation to TPs with low toxicity. The inhibition percentage gradually decreased to 1.6% after 20 min, at which time BPA had been totally removed, and then further to 0.25% after 60 min. The low toxicity is in agreement with the high TOC removal rate (85% after 60 min), indicating the destruction and mineralization of byproducts by the Mn_2O_3/PMS system.

2.6. Comparison between Mn_2O_3 and other Lab-Made Mn-Based Catalysts

The mineralization of the Mn_2O_3/PMS system in the BPA degradation process was investigated based on the removal of TOC. Figure S8 shows that BPA could be fully degraded in 20 min with 79% removal of TOC, and about 94% of TOC could be eliminated in 120 min, which means that the formed TPs could be further degraded by the Mn_2O_3/PMS system. Furthermore, the catalytic performance of the Mn_2O_3 and the previously reported catalysts in PMS activation for BPA degradation were compared.

As listed in Table 1, the Mn_2O_3/PMS system shows superiority in terms of its high TOC removal, low PMS consumption and fast degradation rate for BPA. A fast degradation rate enables short processing time and extensive treatment capacity for continuous flow operation in practical applications. For the next step, our research group will work on field applications of the Mn_2O_3/PMS system by doping catalysts in ceramic membranes as reactive media to enable PMS-based catalytic membrane filtration. How the Mn_2O_3/PMS system responds to real water matrices at large scales will be investigated in the near future.

Table 1. Comparison of catalytic performances of Mn_2O_3 and lab-made catalysts reported in literature.

No.	Catalyst	BPA (mg/L)	PMS (mM)	Catalyst (g/L)	Removal Rate (%)	TOC Removal Rate (%)	Ref.
1	$Mn_{0.8}Fe_{2.2}O_4$	9	0.4	0.1	100 (60 min)	34	[11]
2	CoMnAl	10	0.24	0.02	100 (90 min)	35	[20]
3	MnOx/N-HPCS	10	0.3	0.06	99 (120 min)	39	[22]
4	$MnFe_2O_4$	10	1.0	0.5	88 (90 min)	51	[19]
5	YS-Mn_3O_4	10	0.5	0.1	88 (60 min)	58	[23]
6	Mn/Fe_3O_4	23	2.0	0.2	100 (30 min)	64	[24]
7	$Mn_{0.6}Zn_{0.4}Fe_2O_4$	23	0.5	0.2	96 (60 min)	70	[75]
8	MnFeO	10	0.3	0.1	100 (30 min)	80	[32]
9	$Mn_{1.8}Fe_{1.2}O_4$	10	0.3	0.1	100 (30 min)	80	[32]
10	$BiFeO_3$–MnO_2	50	1.0	0.3	100 (30 min)	85	[81]
11	Mn_2O_3	10	0.1	0.2	100 (20 min)	94	This work

Furthermore, the stability and reusability of the Mn_2O_3 catalysts were investigated. Figure 10 shows that the Mn_2O_3 maintained good catalytic activity after being successively used for eight cycles. BPA removal efficiencies gradually decreased from 100% (the first three tests) to 89% (the eighth test). The gradual decrease in the BPA decontamination rate might have been due to the adsorption of TPs on the surface of Mn_2O_3, the crystal transformation and the loss of manganese [82]. XRD spectra of the fresh and used Mn_2O_3 nanoparticles are shown in Figure S9. No appreciable changes in the characteristic peaks were observed in the XRD spectra, which suggests there was no crystal transformation of the Mn_2O_3 nanoparticles. The concentration of leached Mn ions amounted to around 0.11 mg/L after eight reuses, accounting for only 0.08% of the total Mn content in the catalysts. Therefore, Mn_2O_3 poisoning was the main reason for the activity deficiency. In order to verify this assumption, used Mn_2O_3 catalysts were calcined at 600 °C for 2 h to remove TPs. After calcination, the activity of the Mn_2O_3 was almost recovered. During the ninth test, 99% of the BPA was decomposed in 60 min and 95% of it was removed in 20 min.

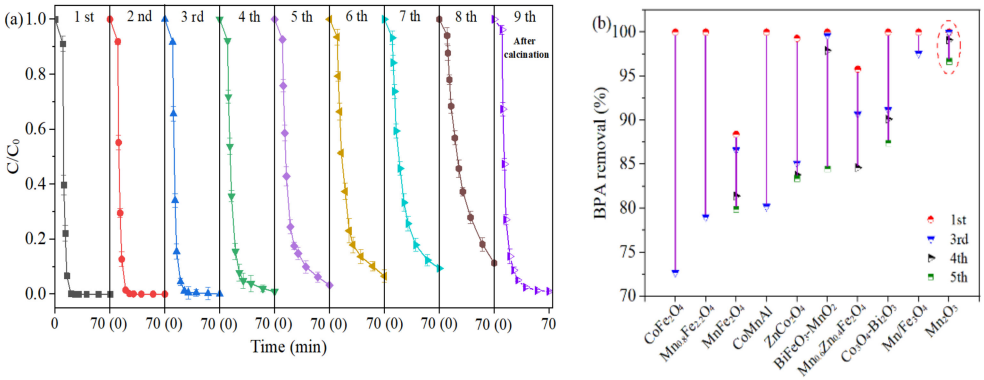

Figure 10. Reusability of Mn_2O_3 and lab-made catalysts reported in literature. (**a**) BPA degradation in eight consecutive runs with the Mn_2O_3/PMS oxidation system (reaction conditions: $[BPA]_0$ = 10 mg/L, $[PMS]_0$ = 0.10 mM, $[Mn_2O_3]_0$ = 0.2 g/L, initial pH = 7.0 ± 0.2, the first 10 min in each cycle was an adsorption stage) and (**b**) the reusability of Mn_2O_3 compared with lab-made catalysts as activators for PMS in the degradation of BPA.

The reusability of Mn_2O_3 was also compared with lab-made catalysts for PMS activation in BPA degradation. As shown in Figure 10b, Mn_2O_3 presented better catalytic abilities, whether after three, four or five cycles, than those of lab-made catalysts such as $MnFe_2O_4$ [19], CoMnAl [20], $CoFe_2O_4$ [21], $Mn_{0.8}Fe_{2.2}O_4$ [11], Mn/Fe_3O_4 [24], $Mn_{0.6}Zn_{0.4}Fe_2O_4$ [75], $BiFeO_3$–MnO_2 [81], $ZnCo_2O_4$ [83] and Co_3O_4-Bi_2O_3 [84]. After eight cycles, the degradation efficiency of BPA in this work was 89%, still higher than that of lab-made catalysts in previous research with less than eight reuse cycles.

3. Materials and Methods

3.1. Chemicals and Materials

The chemicals used in this study are described in the Supporting Information (SI). Mn_2O_3 catalysts with average particle sizes of 1894 nm and 55 nm were purchased from Shanghai Pantian Nano Material Co., Ltd. Mn_2O_3 catalysts with an average particle size of 136 nm were purchased from US Research Nanomaterials, Inc, Houston, TX, USA. Mn_2O_3 catalysts were directly used for experiments without any further treatment.

3.2. Catalytic Degradation Experiments

The catalytic activity of the Mn_2O_3/PMS system was demonstrated by degradation of BPA in aqueous solution. All the degradation experiments were carried out in a 1 L glass beaker. A certain amount of Mn_2O_3 was added to the glass beaker containing 250 mL ultrapure water and sonicated for 10 min to maintain a homogenous solution. Then, the Mn_2O_3 suspension liquid was mixed with a 250 mL solution of 20 mg/L BPA. The reaction mixture was mechanically stirred at 350 rpm for 10 min to reach the absorption equilibrium. NaOH and HNO_3 solutions were used to obtain different initial pH levels for the reaction system. A fixed amount of PMS was added into the mixture to initiate the reaction. Parallel samples were withdrawn at specified time intervals, and then filtered with 0.22 μm polytetrafluoroethylene (PTFE) syringe filters to remove the particles and quenched with methanol before the analysis of BPA concentrations.

For the reusability test of Mn_2O_3 catalysts, the suspension was filtered with 0.22 μm membrane filters after batch experiments, washed with ultrapure water three times and dried in an oven at 80 °C for 24 h before reuse. The experiments in this work were performed in triplicate and the results are represented with mean values and error bars in each graph.

3.3. Analytical Methods

Surface chemical information for Mn_2O_3 was collected via in situ X-ray photoelectron spectroscopy (XPS, PHI-5000, VersaProbeII, ULVAC-PHI, Inc., Chigasaki, Japan) equipped

with an Al kα source, and the binding energies of Mn_2O_3 were calibrated with the C 1 s hydrocarbon peak at 284.80 eV. The X-ray powder diffraction (XRD) spectra of Mn_2O_3 particles were acquired with a Bruker D8 Advance Powder X-ray diffractometer (Bruker, Karlsruhe, Germany) using Cu-kα radiation at 40 kV with 2θ from 20° to 90°. The zeta potential of catalyst particles was determined with a Zeta Sizer (Nano-Z, Malvern Instruments, Worcestershire, UK). The Raman spectra of the samples were obtained with a laser confocal Raman spectrometer (Horiba LabRAM HR800, Piscataway, NJ, USA).

The concentrations of BPA, erythromycin, ofloxacin, paracetamol and naproxen were measured by high performance liquid chromatography-tandem mass spectrometry (HPLC/MS/MS-8050, Shimadzu, Kyoto, Japan), as reported in the literature [85]. The transformation products (TPs) were identified by HPLC/MS/MS equipped with an AQ-C18 HP column (2.1 × 100 mm, 3 μm) using an electro-spray ionization (ESI) source. The TPs were analyzed using ESI on full-scan mode with a mass-to-charge ratio (m/z) from 50 to 450.

The concentration of total organic carbon (TOC) was determined with a TOC analyzer (TOC-VCSH, Shimadzu, Kyoto, Japan) using high temperature combustion. The concentration of PMS was determined using spectrophotometric methods as reported by Wacławek et al. [86]. The amount of leached Mn was measured by ICP/MS (Thermo Scientific iCAP RQ, Bremen, Germany). Electron paramagnetic resonance spectroscopy (EPR) of radical species generated in the Mn_2O_3/PMS system was recorded on a Bruker X-band A200 spectrometer (Karlsruhe, Germany) using DMPO and TMP as spin-trapping agents, respectively. The magnetic field was modulated at 100 kHz, and the power supply was 2.2 mW. The center field was 3480 G with a sweep width of 100 G. The biological toxicities of the BPA and TPs were evaluated through the activated sludge inhibition method according to the procedure that was described in the ISO 8192 method [87].

4. Conclusions

In this study, Mn_2O_3 nanoparticles were applied in activating PMS for the degradation of BPA. Catalytic performances of Mn_2O_3 were comprehensively investigated. The degradation efficiency of 10 mg/L BPA reached as high as 100% within 20 min under the conditions of 0.2 g/L Mn_2O_3 and 0.1 mM PMS. The presence of HCO_3^- and NO_3^- slightly slowed down the degradation kinetics but the degradation efficiency was still kept high. Meanwhile, HA (20 mg/L) presented an obvious inhibiting effect on the degradation of BPA due to the competition of HA with BPA for ROS and with PMS for active sites. Moreover, Mn_2O_3 showed remarkable activity in the activation of PMS and excellent adaptability in various real water matrices, including river water, tap water and secondary effluents. According to the results of the quenching experiment and the EPR results, the non-radical ($^1O_2$) oxidation process played a major role in the degradation of BPA compared to the radical ($O_2^{\bullet-}$/$SO_4^{\bullet-}$/$^{\bullet}$OH) oxidation process. Fifteen transformation products obtained during BPA degradation were studied by HPLC/MS/MS. Dehydroxylation, hydroxylation and β-scission were proposed as three main routes for the degradation pathways of BPA. Compared to lab-made catalysts reported in the literature, the Mn_2O_3 catalyst demonstrated its superiority in terms of its high TOC removal, low PMS consumption, fast degradation rate for BPA and great stability and reusability. Overall, it is easy to conclude from these findings that the Mn_2O_3 catalyst has better applicability than lab-made catalysts for BPA removal in real water.

Supplementary Materials: The following are available online at https://www.mdpi.com/article/10.3390/catal11080993/s1, Figure S1: Zeta potential vs. pH curve of Mn_2O_3, Figure S2: Effects of (a) Cl^-, (b) NO_3^-, (c) HCO_3^-, (d) Ca^{2+}, (e) Mg^{2+} and (f) HA on BPA removal efficiency. Reaction conditions: $[BPA]_0$ = 10 mg/L, $[PMS]_0$ = 0.10 mM, $[Mn_2O_3]_0$ = 0.2 g/L, initial pH = 7.0, Figure S3: In situ Raman spectra of PMS, the commercial Mn_2O_3 and bulk Mn_2O_3/PMS, Figure S4: Homogeneous and heterogeneous catalysis in the degradation of BPA, Figure S5: UV-vis spectra for Mn^{3+}-PP in the reaction solution of the commercial Mn_2O_3/PMS, Figure S6: The total ion current (TIC) chromatogram of TPs and BPA (a); mass spectra of the TPs of the BPA detected in our study (b),

Figure S7: Changes in toxicity with reaction time in the Mn_2O_3/PMS system. Reaction conditions: $[BPA]_0$ = 10 mg/L, $[PMS]_0$ = 0.10 mM, $[Mn_2O_3]_0$ = 0.2 g/L, initial pH = 7.00, Figure S8: TOC removal of BPA by the Mn_2O_3/PMS system. Reaction conditions: $[BPA]_0$ = 10 mg/L, $[PMS]_0$ = 0.10 mM, $[Mn_2O_3]_0$ = 0.2 g/L, initial pH = 7.00, Figure S9: XRD spectra of the fresh and used commercial Mn_2O_3. Table S1: Water quality parameters of real water, Table S2: Main TPs of BPA identified by ESI analysis, Table S3: Identified main TPs of BPA by ESI analysis.

Author Contributions: Conceptualization, L.C.; methodology, L.C.; validation, L.C., W.F. and X.Z.; formal analysis, L.C.; investigation, X.Z.; resources, X.Z; data curation, C.H. and Y.Y.; writing—original draft preparation, L.C.; writing—review and editing, X.Z. and W.F.; supervision, X.Z.; project administration, X.Z.; funding acquisition, X.Z. and W.F. All authors have read and agreed to the published version of the manuscript.

Funding: This research was supported by the China Postdoctoral Science Foundation (Grant No. 2020M680590).

Data Availability Statement: Data sharing not applicable.

Conflicts of Interest: The authors declare no conflict of interest.

References

1. Hu, L.; Zhang, G.; Liu, M.; Wang, Q.; Wang, P. Enhanced degradation of Bisphenol A (BPA) by peroxymonosulfate with Co_3O_4-Bi_2O_3 catalyst activation: Effects of pH, inorganic anions, and water matrix. *Chem. Eng. J.* **2018**, *338*, 300–310. [CrossRef]
2. Hu, Y.; Zhu, Q.; Yan, X.; Liao, C.; Jiang, G. Occurrence, fate and risk assessment of BPA and its substituents in wastewater treatment plant: A review. *Environ. Res.* **2019**, *178*, 108732. [CrossRef]
3. Xiao, C.; Wang, L.; Zhou, Q.; Huang, X. Hazards of bisphenol A (BPA) exposure: A systematic review of plant toxicology studies. *J. Hazard. Mater.* **2019**, *384*, 121488. [CrossRef] [PubMed]
4. Zhang, H.; Zhang, Y.; Li, J.; Yang, M. Occurrence and exposure assessment of bisphenol analogues in source water and drinking water in China. *Sci. Total Environ.* **2018**, *655*, 607–613. [CrossRef] [PubMed]
5. Li, R.-X.; Wang, C.-M.; Cao, J.-k.; Cao, W.-X.; Xu, Q.; Li, J. Monitoring three typical phenol endocrine disrupting compounds in drinking water of Suzhou urban area—From raw water to tap water. *Int. J. Environ. Anal. Chem.* **2018**, *98*, 921–937. [CrossRef]
6. Tang, S.; He, C.; Thai, P.K.; Heffernan, A.; Vijayasarathy, S.; Toms, L.; Thompson, K.; Hobson, P.; Tscharke, B.J.; O'Brien, J.W.; et al. Urinary Concentrations of Bisphenols in the Australian Population and Their Association with the Per Capita Mass Loads in Wastewater. *Environ. Sci. Technol.* **2020**, *54*, 10141–10148. [CrossRef]
7. Olmez-Hanci, T.; Arslan-Alaton, I.; Genc, B. Bisphenol A treatment by the hot persulfate process: Oxidation products and acute toxicity. *J. Hazard. Mater.* **2013**, *263*, 283–290. [CrossRef]
8. Yamazaki, E.; Yamashita, N.; Taniyasu, S.; Lam, J.C.; Lam, P.K.; Moon, H.-B.; Jeong, Y.; Kannan, P.; Achyuthan, H.; Munuswamy, N.; et al. Bisphenol A and other bisphenol analogues including BPS and BPF in surface water samples from Japan, China, Korea and India. *Ecotoxicol. Environ. Saf.* **2015**, *122*, 565–572. [CrossRef] [PubMed]
9. Chen, L.; Fu, W.; Tan, Y.; Zhang, X. Emerging organic contaminants and odorous compounds in secondary effluent wastewater: Identification and advanced treatment. *J. Hazard. Mater.* **2020**, *408*, 124817. [CrossRef]
10. Corrales, J.; Kristofco, L.A.; Steele, W.B.; Yates, B.S.; Breed, C.S.; Williams, E.S.; Brooks, B.W. Global assessment of bisphenol A in the environment: Review and analysis of its occurrence and bioaccumulation. *Dose Response* **2015**, *13*, 1559325815598308. [CrossRef]
11. Qiu, X.; Yang, S.; Dzakpasu, M.; Li, X.; Ding, D.; Jin, P.; Chen, R.; Zhang, Q.; Wang, X. Attenuation of BPA degradation by SO_4^- in a system of peroxymonosulfate coupled with Mn/Fe MOF-templated catalysts and its synergism with Cl^- and bicarbonate. *Chem. Eng. J.* **2019**, *372*, 605–615. [CrossRef]
12. Zhang, Q.; He, D.; Li, X.; Feng, W.; Lyu, C.; Zhang, Y. Mechanism and performance of singlet oxygen dominated peroxymonosulfate activation on CoOOH nanoparticles for 2,4-dichlorophenol degradation in water. *J. Hazard. Mater.* **2019**, *384*, 121350. [CrossRef] [PubMed]
13. Li, C.; Wu, J.; Peng, W.; Fang, Z.; Liu, J. Peroxymonosulfate activation for efficient sulfamethoxazole degradation by Fe_3O_4/β-FeOOH nanocomposites: Coexistence of radical and non-radical reactions. *Chem. Eng. J.* **2018**, *356*, 904–914. [CrossRef]
14. Yang, S.; Wu, P.; Liu, J.; Chen, M.; Ahmed, Z.; Zhu, N. Efficient removal of bisphenol A by superoxide radical and singlet oxygen generated from peroxymonosulfate activated with Fe^0-montmorillonite. *Chem. Eng. J.* **2018**, *350*, 484–495. [CrossRef]
15. Dong, X.; Ren, B.; Sun, Z.; Li, C.; Zhang, X.; Kong, M.; Zheng, S.; Dionysiou, D.D. Monodispersed $CuFe_2O_4$ nanoparticles anchored on natural kaolinite as highly efficient peroxymonosulfate catalyst for bisphenol A degradation. *Appl. Catal. B Environ.* **2019**, *253*, 206–217. [CrossRef]
16. Xue, S.; Li, Q.; Wang, L.; You, W.; Zhang, J.; Che, R. Copper- and Cobalt-Codoped CeO_2 Nanospheres with Abundant Oxygen Vacancies as Highly Efficient Electrocatalysts for Dual-Mode Electrochemical Sensing of MicroRNA. *Anal. Chem.* **2019**, *91*, 2659–2666. [CrossRef] [PubMed]

17. Cai, C.; Kang, S.; Xie, X.; Liao, C.; Duan, X.; Dionysiou, D.D. Efficient degradation of bisphenol A in water by heterogeneous activation of peroxymonosulfate using highly active cobalt ferrite nanoparticles. *J. Hazard. Mater.* **2020**, *399*, 122979. [CrossRef]
18. Hu, P.; Long, M. Cobalt-catalyzed sulfate radical-based advanced oxidation: A review on heterogeneous catalysts and applications. *Appl. Catal. B Environ.* **2016**, *181*, 103–117. [CrossRef]
19. Deng, J.; Xu, M.; Qiu, C.; Chen, Y.; Ma, X.; Gao, N.; Li, X. Magnetic $MnFe_2O_4$ activated peroxymonosulfate processes for degradation of bisphenol A: Performance, mechanism and application feasibility. *Appl. Surf. Sci.* **2018**, *459*, 138–147. [CrossRef]
20. Li, W.; Wu, P.-X.; Zhu, Y.; Huang, Z.; Lu, Y.-H.; Li, Y.-W.; Dang, Z.; Zhu, N.-W. Catalytic degradation of bisphenol A by CoMnAl mixed metal oxides catalyzed peroxymonosulfate: Performance and mechanism. *Chem. Eng. J.* **2015**, *279*, 93–102. [CrossRef]
21. Yang, S.; Qiu, X.; Jin, P.; Dzakpasu, M.; Wang, X.; Zhang, Q.; Zhang, L.; Yang, L.; Ding, D.; Wang, W.; et al. MOF-templated synthesis of $CoFe_2O_4$ nanocrystals and its coupling with peroxymonosulfate for degradation of bisphenol A. *Chem. Eng. J.* **2018**, *353*, 329–339. [CrossRef]
22. Yu, J.; Zhang, J.; Zeng, T.; Wang, H.; Sun, Y.; Chen, L.; Song, S.; Shi, H. Stable incorporation of MnOx quantum dots into N-doped hollow carbon: A synergistic peroxymonosulfate activator for enhanced removal of bisphenol A. *Sep. Purif. Technol.* **2018**, *213*, 264–275. [CrossRef]
23. Zhang, L.; Tong, T.; Wang, N.; Ma, W.; Sun, B.; Chu, J.; Lin, K.-Y.A.; Du, Y. Facile Synthesis of Yolk–Shell Mn_3O_4 Microspheres as a High-Performance Peroxymonosulfate Activator for Bisphenol A Degradation. *Ind. Eng. Chem. Res.* **2019**, *58*, 21304–21311. [CrossRef]
24. Du, J.; Bao, J.; Liu, Y.; Kim, S.H.; Dionysiou, D.D. Facile preparation of porous Mn/Fe_3O_4 cubes as peroxymonosulfate activating catalyst for effective bisphenol A degradation. *Chem. Eng. J.* **2019**, *376*, 119193. [CrossRef]
25. Luo, X.; Liang, H.; Qu, F.; Ding, A.; Cheng, X.; Tang, C.Y.; Li, G. Free-standing hierarchical α-MnO_2@ CuO membrane for catalytic filtration degradation of organic pollutants. *Chemosphere* **2018**, *200*, 237–247. [CrossRef]
26. Lu, S.; Wang, G.; Chen, S.; Yu, H.; Ye, F.; Quan, X. Heterogeneous activation of peroxymonosulfate by $LaCo_{1-x}Cu_xO_3$ perovskites for degradation of organic pollutants. *J. Hazard. Mater.* **2018**, *353*, 401–409. [CrossRef] [PubMed]
27. Yao, Y.; Cai, Y.; Lu, F.; Wei, F.; Wang, X.; Wang, S. Magnetic recoverable MnFe2O4 and $MnFe_2O_4$-graphene hybrid as heterogeneous catalysts of peroxymonosulfate activation for efficient degradation of aqueous organic pollutants. *J. Hazard. Mater.* **2014**, *270*, 61–70. [CrossRef]
28. Tian, N.; Tian, X.; Nie, Y.; Yang, C.; Zhou, Z.; Li, Y. Enhanced 2, 4-dichlorophenol degradation at pH 3–11 by peroxymonosulfate via controlling the reactive oxygen species over Ce substituted 3D Mn_2O_3. *Chem. Eng. J.* **2018**, *355*, 448–456. [CrossRef]
29. Zhang, L.; Zhao, X.; Niu, C.; Tang, N.; Guo, H.; Wen, X.-J.; Liang, C.; Zeng, G. Enhanced activation of peroxymonosulfate by magnetic Co_3MnFeO_6 nanoparticles for removal of carbamazepine: Efficiency, synergetic mechanism and stability. *Chem. Eng. J.* **2019**, *362*, 851–864. [CrossRef]
30. Huang, Y.; Nengzi, L.-C.; Zhang, X.; Gou, J.; Gao, Y.; Zhu, G.; Cheng, Q.; Cheng, X. Catalytic degradation of ciprofloxacin by magnetic $CuS/Fe_2O_3/Mn_2O_3$ nanocomposite activated peroxymonosulfate: Influence factors, degradation pathways and reaction mechanism. *Chem. Eng. J.* **2020**, *388*, 124274. [CrossRef]
31. Deng, J.; Ya, C.; Ge, Y.; Cheng, Y.; Chen, Y.; Xu, M.; Wang, H. Activation of peroxymonosulfate by metal (Fe, Mn, Cu and Ni) doping ordered mesoporous Co_3O_4 for the degradation of enrofloxacin. *RSC Adv.* **2018**, *8*, 2338–2349. [CrossRef]
32. Huang, G.-X.; Wang, C.-Y.; Yang, C.-W.; Guo, P.-C.; Yu, H.-Q. Degradation of Bisphenol A by Peroxymonosulfate Catalytically Activated with $Mn_{1.8}Fe_{1.2}O_4$ Nanospheres: Synergism between Mn and Fe. *Environ. Sci. Technol.* **2017**, *51*, 12611–12618. [CrossRef]
33. Huang, C.; Wang, Y.; Gong, M.; Wang, W.; Mu, Y.; Hu, Z.-H. α-MnO_2/Palygorskite composite as an effective catalyst for heterogeneous activation of peroxymonosulfate (PMS) for the degradation of Rhodamine B. *Sep. Purif. Technol.* **2020**, *230*, 115877. [CrossRef]
34. Chen, G.; Zhang, X.; Gao, Y.; Zhu, G.; Cheng, Q.; Cheng, X. Novel magnetic $MnO_2/MnFe_2O_4$ nanocomposite as a heterogeneous catalyst for activation of peroxymonosulfate (PMS) toward oxidation of organic pollutants. *Sep. Purif. Technol.* **2018**, *213*, 456–464. [CrossRef]
35. Han, M.; Huang, J.; Liang, S.; Shan, L.; Xie, X.; Yi, Z.; Wang, Y.; Guo, S.; Zhou, J. Oxygen Defects in β-MnO_2 Enabling High-Performance Rechargeable Aqueous Zinc/Manganese Dioxide Battery. *Iscience* **2020**, *23*, 100797. [CrossRef]
36. Fang, X.; Xue, Q.; Yu, K.; Li, R.; Jiang, D.; Ge, L.; Ren, Y.; Chen, C.; Wu, X. Superior strength-ductility synergy by hetero-structuring high manganese steel. *Mater. Res. Lett.* **2020**, *8*, 417–423. [CrossRef]
37. Saputra, E.; Muhammad, S.; Sun, H.; Ang, H.-M.; Tadé, M.O.; Wang, S. Manganese oxides at different oxidation states for heterogeneous activation of peroxymonosulfate for phenol degradation in aqueous solutions. *Appl. Catal. B Environ.* **2013**, *142–143*, 729–735. [CrossRef]
38. Deng, J.; Ge, Y.; Tan, C.; Wang, H.; Li, Q.; Zhou, S.; Zhang, K. Degradation of ciprofloxacin using α-MnO_2 activated peroxymonosulfate process: Effect of water constituents, degradation intermediates and toxicity evaluation. *Chem. Eng. J.* **2017**, *330*, 1390–1400. [CrossRef]
39. Matzek, L.W.; Carter, K.E. Activated persulfate for organic chemical degradation: A review. *Chemosphere* **2016**, *151*, 178–188. [CrossRef]
40. Oh, W.-D.; Dong, Z.; Lim, T.-T. Generation of sulfate radical through heterogeneous catalysis for organic contaminants removal: Current development, challenges and prospects. *Appl. Catal. B Environ.* **2016**, *194*, 169–201. [CrossRef]

41. Wang, L.; Jiang, J.; Pang, S.-Y.; Zhou, Y.; Li, J.; Sun, S.; Gao, Y.; Jiang, C. Oxidation of bisphenol A by nonradical activation of peroxymonosulfate in the presence of amorphous manganese dioxide. *Chem. Eng. J.* **2018**, *352*, 1004–1013. [CrossRef]
42. Ren, Y.; Lin, L.; Ma, J.; Yang, J.; Feng, J.; Fan, Z. Sulfate radicals induced from peroxymonosulfate by magnetic ferrospinel MFe_2O_4 (M= Co, Cu, Mn, and Zn) as heterogeneous catalysts in the water. *Appl. Catal. B Environ.* **2015**, *165*, 572–578. [CrossRef]
43. Feng, Y.; Wu, D.; Deng, Y.; Zhang, T.; Shih, K. Sulfate Radical-Mediated Degradation of Sulfadiazine by $CuFeO_2$ Rhombohedral Crystal-Catalyzed Peroxymonosulfate: Synergistic Effects and Mechanisms. *Environ. Sci. Technol.* **2016**, *50*, 3119–3127. [CrossRef] [PubMed]
44. Mady, A.H.; Baynosa, M.L.; Tuma, D.; Shim, J.-J. Heterogeneous activation of peroxymonosulfate by a novel magnetic 3D γ-MnO_2@ $ZnFe_2O_4$/rGO nanohybrid as a robust catalyst for phenol degradation. *Appl. Catal. B Environ.* **2019**, *244*, 946–956. [CrossRef]
45. Huang, Y.-H.; Huang, Y.-F.; Huang, C.-i.; Chen, C.-Y. Efficient decolorization of azo dye Reactive Black B involving aromatic fragment degradation in buffered Co^{2+}/PMS oxidative processes with a ppb level dosage of Co^{2+}-catalyst. *J. Hazard. Mater.* **2009**, *170*, 1110–1118. [CrossRef] [PubMed]
46. Ahmadi, M.; Ghanbari, F. Combination of UVC-LEDs and ultrasound for peroxymonosulfate activation to degrade synthetic dye: Influence of promotional and inhibitory agents and application for real wastewater. *Environ. Sci. Pollut. Res.* **2017**, *25*, 6003–6014. [CrossRef]
47. Oh, W.-D.; Dong, Z.; Hu, Z.-T.; Lim, T.-T. A novel quasi-cubic $CuFe_2O_4$–Fe_2O_3 catalyst prepared at low temperature for enhanced oxidation of bisphenol A via peroxymonosulfate activation. *J. Mater. Chem. A* **2015**, *3*, 22208–22217. [CrossRef]
48. Ghanbari, F.; Moradi, M. Application of peroxymonosulfate and its activation methods for degradation of environmental organic pollutants: Review. *Chem. Eng. J.* **2017**, *310*, 41–62. [CrossRef]
49. Lou, X.; Fang, C.; Geng, Z.; Jin, Y.; Xiao, D.; Wang, Z.; Liu, J.; Guo, Y. Significantly enhanced base activation of peroxymonosulfate by polyphosphates: Kinetics and mechanism. *Chemosphere* **2017**, *173*, 529–534. [CrossRef]
50. Wang, J.; Wang, S. Activation of persulfate (PS) and peroxymonosulfate (PMS) and application for the degradation of emerging contaminants. *Chem. Eng. J.* **2018**, *334*, 1502–1517. [CrossRef]
51. Wu, L.; Zhang, Q.; Hong, J.; Dong, Z.; Wang, J. Degradation of bisphenol A by persulfate activation via oxygen vacancy-rich $CoFe_2O_4$–x. *Chemosphere* **2019**, *221*, 412–422. [CrossRef] [PubMed]
52. Nie, M.; Zhang, W.; Yan, C.; Xu, W.; Wu, L.; Ye, Y.; Hu, Y.; Dong, W. Enhanced removal of organic contaminants in water by the combination of peroxymonosulfate and carbonate. *Sci. Total. Environ.* **2018**, *647*, 734–743. [CrossRef] [PubMed]
53. Mamba, B.; Krause, R.; Malefetse, T.; Sithole, S.; Nkambule, T.T. Humic acid as a model for natural organic matter (NOM) in the removal of odorants from water by cyclodextrin polyurethanes. *Water SA* **2012**, *35*, 117–120. [CrossRef]
54. Wang, S.; Tian, J.; Wang, Q.; Xiao, F.; Gao, S.; Shi, W.; Cui, F. Development of CuO coated ceramic hollow fiber membrane for peroxymonosulfate activation: A highly efficient singlet oxygen-dominated oxidation process for bisphenol a degradation. *Appl. Catal. B Environ.* **2019**, *256*, 117783. [CrossRef]
55. Nie, M.; Deng, Y.; Nie, S.; Yan, C.; Ding, M.; Dong, W.; Dai, Y.; Zhang, Y. Simultaneous removal of bisphenol A and phosphate from water by peroxymonosulfate combined with calcium hydroxide. *Chem. Eng. J.* **2019**, *369*, 35–45. [CrossRef]
56. Wang, H.; Liu, Z.-H.; Zhang, J.; Huang, R.-P.; Yin, H.; Dang, Z.; Wu, P.-X.; Liu, Y. Insights into removal mechanisms of bisphenol A and its analogues in municipal wastewater treatment plants. *Sci. Total Environ.* **2019**, *692*, 107–116. [CrossRef]
57. Zhu, S.; Li, X.; Kang, J.; Duan, X.; Wang, S. Persulfate Activation on Crystallographic Manganese Oxides: Mechanism of Singlet Oxygen Evolution for Nonradical Selective Degradation of Aqueous Contaminants. *Environ. Sci. Technol.* **2018**, *53*, 307–315. [CrossRef]
58. Jawad, A.; Lu, X.; Chen, Z.; Yin, G. Degradation of Chlorophenols by Supported Co–Mg–Al Layered Double Hydrotalcite with Bicarbonate Activated Hydrogen Peroxide. *J. Phys. Chem. A* **2014**, *118*, 10028–10035. [CrossRef]
59. Xie, M.; Tang, J.; Kong, L.; Lu, W.; Natarajan, V.; Zhu, F.; Zhan, J. Cobalt doped g-C_3N_4 activation of peroxymonosulfate for monochlorophenols degradation. *Chem. Eng. J.* **2018**, *360*, 1213–1222. [CrossRef]
60. Fontmorin, J.; Castillo, R.B.; Tang, W.; Sillanpää, M. Stability of 5, 5-dimethyl-1-pyrroline-N-oxide as a spin-trap for quantification of hydroxyl radicals in processes based on Fenton reaction. *Water Res.* **2016**, *99*, 24–32. [CrossRef]
61. Khan, A.; Wang, H.; Liu, Y.; Jawad, A.; Ifthikar, J.; Liao, Z.; Wang, T.; Chen, Z. Highly efficient α-Mn_2O_3@ α-MnO_2-500 nanocomposite for peroxymonosulfate activation: Comprehensive investigation of manganese oxides. *J. Mater. Chem. A* **2018**, *6*, 1590–1600. [CrossRef]
62. Ma, Q.; Pei, Y.; Dai, D.; Peng, X.; Cui, D.; Liu, C.; Yuan, L. Core-shell structured Mn_2O_3/MgO microsphere for removal of C.I. Basic Violet 3 from aqueous solution. *Colloids Surfaces A Physicochem. Eng. Asp.* **2018**, *545*, 188–196. [CrossRef]
63. Yu, J.; Zeng, T.; Wang, H.; Zhang, H.; Sun, Y.; Chen, L.; Song, S.; Li, L.; Shi, H. Oxygen-defective MnO_2-x rattle-type microspheres mediated singlet oxygen oxidation of organics by peroxymonosulfate activation. *Chem. Eng. J.* **2020**, *394*, 124458. [CrossRef]
64. Zhang, T.; Li, W.; Croué, J.-P. Catalytic Ozonation of Oxalate with a Cerium Supported Palladium Oxide: An Efficient Degradation Not Relying on Hydroxyl Radical Oxidation. *Environ. Sci. Technol.* **2011**, *45*, 9339–9346. [CrossRef] [PubMed]
65. Cheng, Y.; Zhang, G.; Liu, H.; Qu, J. Confining Free Radicals in Close Vicinity to Contaminants Enables Ultrafast Fenton-like Processes in the Interspacing of MoS_2 Membranes. *Angew. Chem. Int. Ed.* **2019**, *58*, 8134–8138. [CrossRef] [PubMed]
66. Webb, S.M.; Dick, G.; Bargar, J.R.; Tebo, B.M. Evidence for the presence of Mn(III) intermediates in the bacterial oxidation of Mn(II). *Proc. Natl. Acad. Sci. USA* **2005**, *102*, 5558–5563. [CrossRef]

67. Zhao, B.; Ran, R.; Wu, X.; Weng, D. Phase structures, morphologies, and NO catalytic oxidation activities of single-phase MnO2 catalysts. *Appl. Catal. A Gen.* **2016**, *514*, 24–34. [CrossRef]
68. Tan, X.; Wan, Y.; Huang, Y.; He, C.; Zhang, Z.; He, Z.; Hu, L.; Zeng, J.; Shu, D. Three-dimensional MnO_2 porous hollow microspheres for enhanced activity as ozonation catalysts in degradation of bisphenol A. *J. Hazard. Mater.* **2017**, *321*, 162–172. [CrossRef]
69. Li, C.; Huang, Y.; Dong, X.; Sun, Z.; Duan, X.; Ren, B.; Zheng, S.; Dionysiou, D.D. Highly efficient activation of peroxymonosulfate by natural negatively-charged kaolinite with abundant hydroxyl groups for the degradation of atrazine. *Appl. Catal. B Environ.* **2019**, *247*, 10–23. [CrossRef]
70. Zhang, B.; Wang, L.; Zhang, Y.; Ding, Y.; Bi, Y. Ultrathin FeOOH Nanolayers with Abundant Oxygen Vacancies on $BiVO_4$ Photoanodes for Efficient Water Oxidation. *Angew. Chem. Int. Ed.* **2018**, *57*, 2248–2252. [CrossRef]
71. Gao, R.; Zhang, D.; Maitarad, P.; Shi, L.; Rungrotmongkol, T.; Li, H.; Zhang, J.; Cao, W. Morphology-dependent properties of MnO x/ZrO_2–CeO_2 nanostructures for the selective catalytic reduction of NO with NH_3. *J. Phys. Chem. C* **2013**, *117*, 10502–10511. [CrossRef]
72. Liu, Y.; Guo, H.; Zhang, Y.; Tang, W.; Cheng, X.; Li, W. Heterogeneous activation of peroxymonosulfate by sillenite $Bi_{25}FeO_{40}$: Singlet oxygen generation and degradation for aquatic levofloxacin. *Chem. Eng. J.* **2018**, *343*, 128–137. [CrossRef]
73. Tan, C.; Gao, N.; Fu, D.; Deng, J.; Deng, L. Efficient degradation of paracetamol with nanoscaled magnetic $CoFe_2O_4$ and $MnFe_2O_4$ as a heterogeneous catalyst of peroxymonosulfate. *Sep. Purif. Technol.* **2017**, *175*, 47–57. [CrossRef]
74. Li, Y.; Li, D.; Fan, S.; Yang, T.; Zhou, Q. Facile template synthesis of dumbbell-like Mn_2O_3 with oxygen vacancies for efficient degradation of organic pollutants by activating peroxymonosulfate. *Catal. Sci. Technol.* **2020**, *10*, 864–875. [CrossRef]
75. Lin, H.; Li, S.; Deng, B.; Tan, W.; Li, R.; Xu, Y.; Zhang, H. Degradation of bisphenol A by activating peroxymonosulfate with $Mn^{0.6}Zn_{0.4}Fe_2O_4$ fabricated from spent Zn-Mn alkaline batteries. *Chem. Eng. J.* **2019**, *364*, 541–551. [CrossRef]
76. Kim, H.; Kim, W.; Mackeyev, Y.; Lee, G.-S.; Kim, H.-J.; Tachikawa, T.; Hong, S.; Lee, S.; Kim, J.; Wilson, L.J.; et al. Selective Oxidative Degradation of Organic Pollutants by Singlet Oxygen-Mediated Photosensitization: Tin Porphyrin versus C60 Aminofullerene Systems. *Environ. Sci. Technol.* **2012**, *46*, 9606–9613. [CrossRef] [PubMed]
77. Ding, Y.; Zhou, P.; Tang, H. Visible-light photocatalytic degradation of bisphenol A on $NaBiO_3$ nanosheets in a wide pH range: A synergistic effect between photocatalytic oxidation and chemical oxidation. *Chem. Eng. J.* **2016**, *291*, 149–160. [CrossRef]
78. Zhang, H.; Huang, C.-H. Reactivity and Transformation of Antibacterial N-Oxides in the Presence of Manganese Oxide. *Environ. Sci. Technol.* **2004**, *39*, 593–601. [CrossRef]
79. Zhang, M.; Xiao, C.; Yan, X.; Chen, S.; Wang, C.; Luo, R.; Qi, J.; Sun, X.; Wang, L.; Li, J. Efficient Removal of Organic Pollutants by Metal–organic Framework Derived Co/C Yolk–Shell Nanoreactors: Size-Exclusion and Confinement Effect. *Environ. Sci. Technol.* **2020**, *54*, 10289–10300. [CrossRef]
80. Lin, K.; Liu, W.; Gan, J. Oxidative Removal of Bisphenol A by manganese dioxide efficacy, products and pathway. *Environ. Sci. Technol.* **2009**, *43*, 3860–3864. [CrossRef]
81. Li, L.; Liu, Y.; Zhang, S.; Liang, M.; Li, F.; Yuan, Y. Enhanced mineralization of bisphenol A by eco-friendly $BiFeO_3$–MnO_2 composite: Performance, mechanism and toxicity assessment. *J. Hazard. Mater.* **2020**, *399*, 122883. [CrossRef] [PubMed]
82. Sun, P.H.; Liang, H.; Zhou, G.; Wang, S. Supported cobalt catalysts by one-pot aqueous combustion synthesis for catalytic phenol degradation. *J. Colloid Interface Sci.* **2012**, *394*, 394–400. [CrossRef] [PubMed]
83. Hu, L.; Zhang, G.; Liu, M.; Wang, Q.; Wang, P.J. Optimization of the catalytic activity of a $ZnCo_2O_4$ catalyst in peroxymonosulfate activation for bisphenol A removal using response surface methodology. *Chemosphere* **2018**, *212*, 152–161. [CrossRef] [PubMed]
84. Hu, L.; Zhang, G.; Liu, M.; Wang, Q.; Dong, S.; Wang, P. Application of nickel foam-supported Co_3O_4-Bi_2O_3 as a heterogeneous catalyst for BPA removal by peroxymonosulfate activation. *Sci. Total Environ.* **2018**, *647*, 352–361. [CrossRef]
85. Wang, L.Y.; Zhang, X.H.; Tam, N.F.-Y. Analysis and occurrence of typical endocrine-disrupting chemicals in three sewage treatment plants. *Water Sci. Technol.* **2010**, *62*, 2501–2509. [CrossRef]
86. Wacławek, S.; Lutze, H.; Grübel, K.; Padil, V.V.T.; Černík, M.; Dionysiou, D. Chemistry of persulfates in water and wastewater treatment: A review. *Chem. Eng. J.* **2017**, *330*, 44–62. [CrossRef]
87. Arslan-Alaton, I.; Ayten, N.; Olmez-Hanci, T. Photo-Fenton-like treatment of the commercially important H-acid: Process optimization by factorial design and effects of photocatalytic treatment on activated sludge inhibition. *Appl. Catal. B Environ.* **2010**, *96*, 208–217. [CrossRef]